Solar Energy 196 (2020) 457–461

Contents lists available at ScienceDirect

Solar Energy

journal homepage: www.elsevier.com/locate/solener

Effect of strain on the dark current-voltage characteristic of silicon heterojunction solar cells

L. Guin[a,b,1], P. Roca i Cabarrocas[b,*], M.E. Jabbour[a,c], N. Triantafyllidis[a,c,d]

[a] LMS, École polytechnique, CNRS, Institut polytechnique de Paris, 91128 Palaiseau, France
[b] LPICM, École polytechnique, CNRS, Institut polytechnique de Paris, 91128 Palaiseau, France
[c] Département de Mécanique, École polytechnique, 91128 Palaiseau, France
[d] Aerospace Engineering Department & Mechanical Engineering Department (emeritus), The University of Michigan, Ann Arbor, MI 48109-2140, USA

ARTICLE INFO

Keywords:
Strain effect
Stress
Mechanical loading
Solar cell
Piezojunction effect

ABSTRACT

Anisotropic mechanical strain as low as 0.1% modifies the electronic response of crystalline semiconductor-based devices and in particular affects the performance of solar cells. We measure the dark current-voltage characteristic of silicon heterojunction solar cells under different levels of tensile uniaxial stress and observe a reversible change of the *j-V* curve with applied strain. Using a two-exponential description of the *j-V* characteristic to fit our experimental data, we obtain the strain dependence of the diffusion saturation current and find a decrease of about 3% for a tensile strain level of 6.7×10^{-4}. We compare these experiments to a theoretical model that accounts for the effect of strain on the band energy levels, densities of states and mobilities of carriers. The theoretical estimation of the change in saturation current is found to be in reasonable agreement with experimental results.

1. Introduction

Mechanical anisotropic strain, by breaking the symmetry of the atomic lattice, modifies the electronic properties of crystalline semiconductors. In crystalline silicon, the strain dependence of these electronic properties has been investigated both theoretically for the band energy levels and densities of states of the conduction and valence bands through deformation potential theory (Bardeen and Shockley, 1950; Herring and Vogt, 1956; Bir et al., 1974; Fischetti and Laux, 1996; Creemer, 2002) and experimentally for the mobilities of carriers (Smith, 1954; Kanda, 1991; Kleimann et al., 1998; Lange et al., 2016). At the macroscale, strain modifies the electronic response of electronic devices such as *p-n* junctions (Wortman et al., 1964; Wortman and Hauser, 1966; Kanda, 1967; Rueda, 1999) and transistors (Creemer and French, 2000; Creemer et al., 2001; Creemer, 2002), a phenomenon called the *piezojunction effect*. In the early experimental studies of this effect on *p-n* junctions (Imai et al., 1965; Rindner, 1965; Wooten et al., 1968), strains were applied through an indenter tip or by bonding the device to a substrate subjected to deformations, which introduced complex strain spatial distributions and uncertainties in the strain field that develops in the device. While for the high level of stress (~1 GPa) exerted in these experiments, the predominant mechanism in the piezojunction effect is the change in band energy levels (Wortman et al., 1964; Wortman and Hauser, 1966; Kanda, 1967), more sophisticated models are necessary for lower levels of stress, as typically encountered in real applications. Indeed, for moderate stress levels in transistors (~100 MPa), Creemer and French (2000) pointed out that the strain dependences of the band energy levels, densities of states, and mobilities have comparable contributions to the piezojunction effect.

Solar cells are a large domain of application of *p-n* junctions, where stresses may be encountered both during the fabrication process and in device use, in particular with emerging flexible solar cells (Pagliaro et al., 2008; Velut et al., 2014). Existing works on the effect of stress on the performance of solar cells concern amorphous silicon solar cells and are limited to experimental investigations (Jones et al., 2002; Gleskova et al., 2006; Chen et al., 2018; Dai et al., 2019). Indeed, because the strain-dependence of the electronic properties of amorphous materials is currently not well known, the modeling of the effect of stress on the electronic response of devices based on these materials remains difficult. By contrast, with crystalline-based solar cells, one may use the extensive knowledge on the strain-dependence of the properties of crystalline silicon to develop an understanding of the mechanisms underlying the effect of strain on their electronic response. This is what we propose in the present work by investigating both experimentally and

* Corresponding author.
E-mail address: pere.roca@polytechnique.edu (P. Roca i Cabarrocas).
[1] Present address: Mechanics & Materials, Department of Mechanical and Process Engineering, ETH Zürich, Zürich 8092, Switzerland.

https://doi.org/10.1016/j.solener.2019.12.037
Received 3 October 2019; Received in revised form 10 December 2019; Accepted 13 December 2019
Available online 24 December 2019
0038-092X/

through modeling the strain-induced changes in the electronic reponse of silicon heterojunction solar cells.

The rest of the article is organized as follows. In Section 2, we present the experimental pocedure consisting of the fabrication of Silicon HeteroJunction (SHJ) solar cells and the setup used for the combined electro-mechanical measurements. Experimental results on the strain dependence of the *j-V* curve under uniaxial tension are given in Section 3, whereas a theoretical model for this effect is proposed in Section 4. Finally, we draw concluding remarks in Section 5.

2. Experimental

2.1. Silicon heterojunction solar cells

The SHJ solar cells used in the experiments are fabricated from a commercial (100) n-doped c-Si wafer of resistivity 2.6 Ω·cm. After dipping the wafer for 30 s in a solution of 5% HF, a-SiC:H and a:Si-H layers are deposited by Plasma-Enhanced Chemical Vapor Deposition (PECVD) at 175 °C. Aluminum electrodes are subsequently deposited by thermal evaporation in vacuum and the resulting cells are annealed at 180 °C for 15 min to improve the carrier lifetime. The resulting structure of the solar cell is shown on Fig. 1. Note that, for the evaporation of the top electrode, we use a mask with square cell sections of 5×5 mm^2 with sides oriented along the $\langle 110 \rangle$ directions. After fabrication, the cells are separated by cutting 15×15 mm^2 squares providing space around each cell for gripping it throughout the mechanical loading.

2.2. Setup for mechanical loading

To load mechanically the solar cells, we use an Instron 3366 electromechanical testing machine with home-made three-dimensional printed grips. As depicted in Fig. 2, the 15×15 mm^2 and 270 μm thick solar cell is glued inside the 500 μm grooves of the polymer grips. Note that the sample is glued after the grips have been set in the testing machine in order to avoid exerting pre-stress on the silicon wafer.

In such a configuration, the silicon sample carries all the uniaxial load exerted by the testing machine. Moreover, given that the stiffness of the polymer grips (Young's modulus is about 2.4 GPa) is much smaller than that of silicon (elastic coefficients of the order of 100 GPa), we can assume the silicon wafer to be in a state of uniaxial stress. Using the elastic properties of silicon (described by the elasticity tensor $\mathbf{c}$ of silicon Wortman and Evans, 1965), we can derive its strain state (described by the small strain tensor $\boldsymbol{\varepsilon}$) from the load F measured by the load cell of the testing machine with

$$\boldsymbol{\varepsilon} = \mathbf{c}^{-1} : \boldsymbol{\sigma}, \tag{1}$$

where the stress state $\boldsymbol{\sigma}$ is approximately given by

$$\boldsymbol{\sigma} = \frac{F}{S} \mathbf{e}_y \otimes \mathbf{e}_y, \tag{2}$$

with $\mathbf{e}_y$ the loading direction (cf. Fig. 2) and S the section area of the silicon sample in the $(\mathbf{e}_x, \mathbf{e}_z)$ plane.

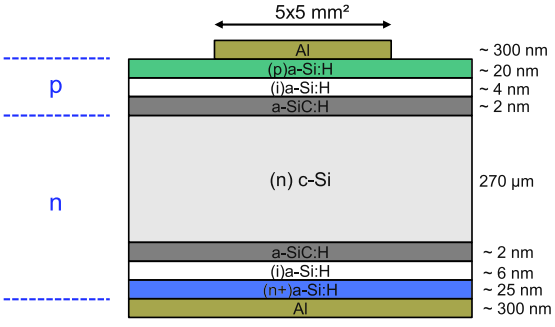

Fig. 1. Structure of the silicon heterojunction solar cell.

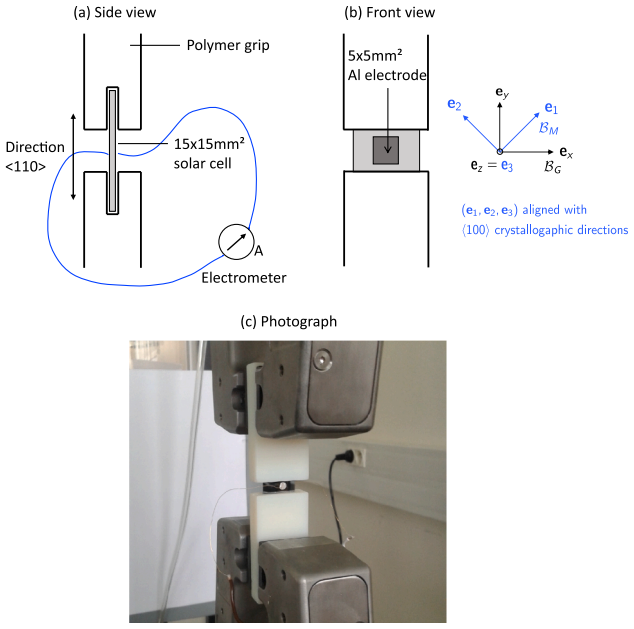

Fig. 2. Schematic [(a) and (b)] and photograph (c) of the experimental set-up, with the 15×15 mm^2 solar cell glued inside the grooves of polymer grips. $\mathcal{B}_M = (\mathbf{e}_1, \mathbf{e}_2, \mathbf{e}_2)$ (M for material) is an orthonormal basis aligned with the $\langle 100 \rangle$ directions of the crystal; $\mathcal{B}_G = (\mathbf{e}_x, \mathbf{e}_y, \mathbf{e}_z)$ (G for grips) is obtained by rotating $\mathcal{B}_M$ by $\pi/4$ in the clockwise direction and has its vector $\mathbf{e}_y$ aligned with the loading direction.

2.3. Electrical measurements

For the electrical measurements, the solar cell is connected to a Keithley 2460 sourcemeter using gold wires bonded with silver paste to its front and back electrodes. With this set-up, the current-voltage characteristic of the solar cell is measured for different loading forces: $F = 200$ N ($\varepsilon_{yy} = 2.7 \times 10^{-4}$), $F = 300$ N ($\varepsilon_{yy} = 4.1 \times 10^{-4}$), $F = 400$ N ($\varepsilon_{yy} = 5.4 \times 10^{-4}$), and $F = 500$ N ($\varepsilon_{yy} = 6.8 \times 10^{-4}$), which is the last level of loading before the failure of the sample. At the different load levels, the displacement of the grips is maintained fixed for about one minute, which is the time needed to measure the *j-V* characteristic. Note that, in order to check the reversibility with deformation of the change in the characteristic, we return to zero load ($F = 0$) between the different loading levels and measure, in these relaxed states, the *j-V* characteristics.

3. Results

3.1. Dark current-voltage characteristics under mechanical loading

Fig. 3 shows the current-voltage characteristic of a particular solar cell for different levels of applied strain. At the scale of Fig. 3(a), the *j-V* curves superimpose and the effect of strain is not visible; we therefore plot them in Fig. 3(b) in the restricted voltage range 0.381 V – 0.383 V. Curves 1 and 2 at zero-strain are two measurements performed with an interval of 12 h, the drying time for the glue. Curves 3 and 4 display a shift in characteristic induced by the first two strain levels and Curve 5 at zero-strain shows a small residual irreversible part in the mechanically-induced change. Moreover, whereas changes with further increments of strain are displayed by Curves 6 and 8, one can see on Curve 7 at zero-strain that the residual change observed in step 5 has not increased. Hence, while the first level of loading may have induced some irreversible change in the cell, most of the contribution to the strain-induced change is indeed due to elastic deformation of the semiconductor.

Note that our experimental results agree well with those performed

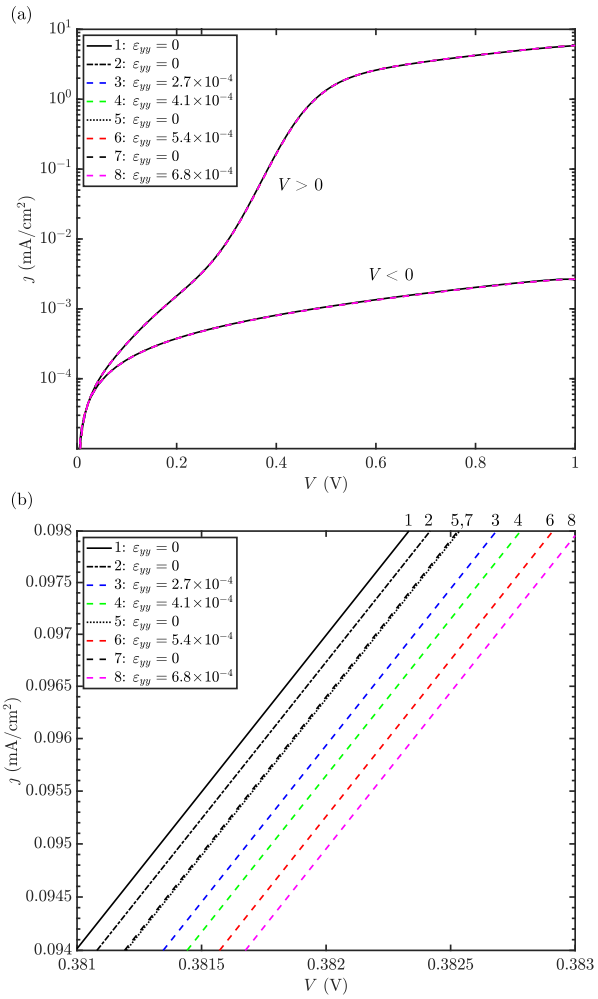

Fig. 3. Current-voltage characteristics of a SHJ solar cell under different levels of applied strain. In (a) the voltage ranges from − 1 V to 1 V, whereas (b) is a zoom on the range 0.381 V – 0.383 V. Numbers 1 to 8 indicate the chronological order of mechanical loadings and unloadings.

by Rueda (1999) on purely crystalline silicon *p-n* junctions in the context of integrated circuit. In that work, the author used a four-point bending flexural test to measure the effect of both compressive and tensile stress on the *j-V* characteristic of planar and lateral *p-n* junctions. Notwithstanding the difference with our experimental set-up, in that the four-point bending induces a non-uniform strain field, these measurements of the decrease in the direct current under tensile strain are comparable to ours.

3.2. Strain dependence of the diffusion saturation current

In order to quantify the strain dependence of the parameters of the cell, in particular of the diffusion saturation current $j_s(\varepsilon)$, we use a two-exponential model (Wolf et al., 1977; Suckow et al., 2012) of the *j-V* relation with effective series resistance $R_s(\varepsilon)$ and parallel resistance $R_p(\varepsilon)$ to fit the experimental data:

$$j = \underbrace{j_s(\varepsilon)\left(\exp\left(\frac{q(V-jR_s(\varepsilon))}{k_BT}\right)-1\right)}_{\text{Diffusion current}} + \underbrace{j_r(\varepsilon)\left(\exp\left(\frac{q(V-jR_s(\varepsilon))}{2k_BT}\right)-1\right)}_{\text{Recombination-generation current}} + \underbrace{\frac{V-jR_s(\varepsilon)}{R_p(\varepsilon)}}_{\text{Parallel resistance current}}, \quad (3)$$

with $j_r(\varepsilon)$ the saturation current of the Recombination-Generation (RG) current (Sze and Ng, 2006), q the elementary charge, k_B the Boltzmann constant and T the absolute temperature. The equivalent electric circuit corresponding to the two-exponential model (3) is shown on Fig. 4.

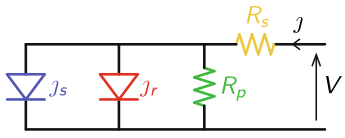

Fig. 4. Equivalent electric circuit for the two-exponential model with *j-V* expression (3).

Note that, in contrast with j_s, we do not have physical models for the dependence of j_r, R_s, and R_p on strain. Indeed, R_s and R_p are phenomenological quantities introduced to account for the parasitic resistances of various physical origins (e. g., contact resistance, resistance of the semiconductor layers, shunts). Likewise, since j_r is associated with recombination in the space charge region, it involves electronic properties of both the crystalline and amorphous silicon, and the strain dependence of the latter is unknown.

To determine the four model parameters j_s, j_r, R_s and R_p from the experimental *j-V* characteristics, we use the algorithm developed by Suckow et al. (2012) (see also Suckow, 2014) based on a least-square fit of Eq. (3) to the experimental data. The parameters obtained from the *j-V* curve of Fig. 3 are summarized in Table 1. Thereafter, the strain dependence of the cell parameters is obtained by carrying out, at the different loading steps, two different fitting procedures as follows:

1. *Fit 1*: In the first procedure, the fit is performed over the range (−1 V, 1 V) with respect to the four parameters j_s, j_r, R_s and R_p, for all the loading levels.
2. *Fit 2*: For comparison, we use a second fitting procedure restricted to the range (0.2 V, 0.5 V) with R_s and R_p kept fixed across the fits at different loading levels. Indeed, since, in this range, j_s contributes predominantly to the total current, it corresponds to the region where there is most of the information on it.

The relative changes in j_s, as defined by $\Delta j_s(\varepsilon) = (j_s(\varepsilon) - j_s(\mathbf{0}))/j_s(\mathbf{0})$, are reported on Fig. 5. One can see a relative change in the diffusion saturation current of about − 3% for a strain of ~7×10^{-4}. The difference between the two methods gives an idea of the uncertainty on that measurement, which is about 1% in absolute value.

4. Modeling of the strain-effect

To interpret the measurements of the strain-induced change in the diffusion saturation current, we use a model accounting for the strain dependence of the following electronic properties of silicon: band energy levels ($E_c(\varepsilon)$ and $E_v(\varepsilon)$) and densities of states ($N_c(\varepsilon)$ and) of the conduction and valence bands, as well as mobilities ($m_n(\varepsilon)$ and $m_p(\varepsilon)$) of electrons and holes (Guin et al., 2018; Guin, 2018). We model the solar cell as a *p-n* heterojunction with *p-* and *n*-doped regions—corresponding to the (p) a-Si:H layer and (n) c-Si wafer, cf. Fig. 1—with thicknesses W_p and W_n, respectively. Note that the intrinsic amorphous silicon, *n*-doped amorphous silicon, and silicon carbide layers that are part of the solar cell structure shown on Fig. 1 are buffer and passivation layers which are not explicitly modeled. However, the

Table 1
Best fit parameters of (3) with the experimental *j-V* characteristic of the solar cell of Fig. 3 for a fit over the range (−1 V, 1 V).

j_s (mA/cm^2)	j_r (mA/cm^2)	R_s (Ω·cm^2)	R_p (Ω·cm^2)
3.7×10^{-8}	1.5×10^{-5}	71	4.9×10^{5}

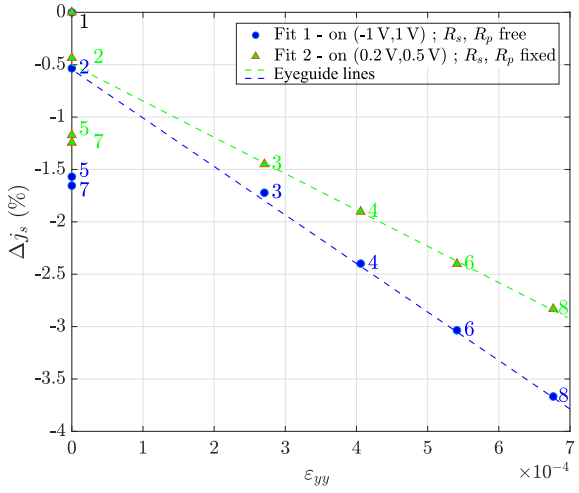

Fig. 5. Relative change $\Delta j_s = (j_s(\boldsymbol{\varepsilon}) - j_s(\boldsymbol{0}))/j_s(\boldsymbol{0})$ of the diffusion saturation current associated with the *j-V* curves of Fig. 3 with the two fitting procedures Fit 1 and Fit 2.

influence of these layers on the electric response appears through the effective surface recombination velocities S_n on the front side (top of (p) a-Si:H layer) and S_p on the back side (bottom of (n) c-Si layer). Let τ_n and τ_p be the carrier lifetimes and denote by $L_n(\boldsymbol{\varepsilon}) = \sqrt{U_T m_n(\boldsymbol{\varepsilon})\tau_n}$ and $L_p(\boldsymbol{\varepsilon}) = \sqrt{U_T m_p(\boldsymbol{\varepsilon})\tau_p}$ the associated diffusion lengths where $U_T = k_B T/q$ is the thermal voltage. Note that our focus being on the strain-induced changes in the current, only relative changes in currents and not their absolute values are relevant. As a result, as long as surface recombination velocities and carrier lifetimes are supposed independent of strain, their values are not needed. The expression of the diffusion saturation current is a generalization of the Shockley relation (Nelson, 2003; Fonash, 2012):

$$j_s = j_{sn} + j_{sp}, \tag{4}$$

where j_{sn} and j_{sp} are the contributions to the diffusion saturation current of the layers (p) a-Si:H and (n) c-Si, respectively, with expressions:

$$\begin{aligned} j_{sn} &= q(n_i^a)^2 \frac{U_T m_n}{N_a L_n} \frac{\frac{L_n S_n}{U_T m_n}\cosh(W_p/L_n) + \sinh(W_p/L_n)}{\frac{L_n S_n}{U_T m_n}\sinh(W_p/L_n) + \cosh(W_p/L_n)}, \\ j_{sp} &= q(n_i^c)^2 \frac{U_T m_p}{N_d L_p} \frac{\frac{L_p S_p}{U_T m_p}\cosh(W_n/L_p) + \sinh(W_n/L_p)}{\frac{L_p S_p}{U_T m_p}\sinh(W_n/L_p) + \cosh(W_n/L_p)}, \end{aligned} \tag{5}$$

where N_a and N_d are the acceptor and donor dopant concentrations, and $n_i^a(\boldsymbol{\varepsilon})$ and $n_i^c(\boldsymbol{\varepsilon})$ are the intrinsic carrier concentrations in the (p) a-Si:H layer and (n) c-Si wafer, respectively. The latter involve the density of states and band gap $E_{gap}(\boldsymbol{\varepsilon}) = E_c(\boldsymbol{\varepsilon}) - E_v(\boldsymbol{\varepsilon})$ for amorphous and crystalline silicon according to:

$$\begin{aligned} (n_i^a)^2 &= N_c^a N_v^a \exp[-E_{gap}^a/k_B T], \\ (n_i^c)^2 &= N_c^c N_v^c \exp[-E_{gap}^c/k_B T], \end{aligned} \tag{6}$$

where the superscripts a and c are associated to the amorphous and crystalline layers, respectively. Given the state of homogeneous strain to which the cell is subjected, the change with strain of j_s can be directly computed from Eqs. (4) and (5) using the strain dependence of the band energy levels, densities of states and carrier mobilities.

Experiments measuring the temperature dependence of j_s in SHJ solar cells similar to ours (Taguchi et al., 2008) yield an exponential dependence with $-1/T$ with an activation energy of 1.13 eV. This value, which corresponds to the band gap of crystalline silicon, indicates that the component j_{sp} coming from the crystalline wafer is predominant in Eq. (4), that is,

$$j_s(\boldsymbol{\varepsilon}) \approx j_{sp}(\boldsymbol{\varepsilon}). \tag{7}$$

It turns out that for the particular crystallographic directions chosen in the experiments (uniaxial stress along direction ⟨110⟩ and current and voltage along direction ⟨100⟩ as shown on Fig. 2), the strain dependence in the hole mobility can be neglected (see details in the Supplementary Material). Moreover, N_c in silicon has also a negligible dependence on strain (Kanda, 1967; Bir et al., 1974; Kleimann et al., 1998; Creemer, 2002). As a result, the saturation current simplifies to

$$\begin{aligned} j_s(\boldsymbol{\varepsilon}) = {} & q N_c^c N_v^c(\boldsymbol{\varepsilon}) \exp[-(E_c^c(\boldsymbol{\varepsilon}) - E_v^c(\boldsymbol{\varepsilon}))/k_B T] \times \\ & \frac{U_T m_p}{N_d L_p} \frac{\frac{L_p S_p}{U_T m_p}\cosh(W_n/L_p) + \sinh(W_n/L_p)}{\frac{L_p S_p}{U_T m_p}\sinh(W_n/L_p) + \cosh(W_n/L_p)}, \end{aligned} \tag{8}$$

where, in Eq. (8), the significant dependences of the electronic parameters on $\boldsymbol{\varepsilon}$ have been explicitly written. In turn, the relative change in saturation current with strain can be linearized as

$$\Delta j_s(\boldsymbol{\varepsilon}) = \frac{j_s(\boldsymbol{\varepsilon}) - j_s(\boldsymbol{0})}{j_s(\boldsymbol{0})} = -\frac{\Delta E_c^c(\boldsymbol{\varepsilon})}{k_B T} + \frac{\Delta E_v^c(\boldsymbol{\varepsilon})}{k_B T} + \frac{\Delta N_v^c(\boldsymbol{\varepsilon})}{N_v^c(\boldsymbol{0})}. \tag{9}$$

Numerically, with the strain state of the experiment given by Eq. (1), we obtain for $\varepsilon_{yy} = 6.8 \times 10^{-4}$ (cf. the Supplementary Material for the expressions of the strain-dependent electronic parameters $E_c^c(\boldsymbol{\varepsilon})$, $E_v^c(\boldsymbol{\varepsilon})$ and $N_v^c(\boldsymbol{\varepsilon})$),

$$\Delta j_s = \underbrace{-7\%}_{-\frac{\Delta E_c^c}{k_B T}} \underbrace{+7\%}_{\frac{\Delta E_v^c}{k_B T}} \underbrace{-6\%}_{\frac{\Delta N_v^c}{N_v^c}} = -6\%. \tag{10}$$

The change in saturation current of -6% predicted by the theory is about twice what we have measured. From the decomposition Eq. (10), we can see that the predicted variation of -6% results from the combination of the positive and negative effects of the various parameters, among which the effect of strain on the density of states of the valence band. It is likely that the discrepancy between the experimental result and the modeling essentially comes from the limited knowledge of the strain dependence $N_v(\boldsymbol{\varepsilon})$. Indeed, while this parameter has a significant contribution to the total change in saturation current, the dependence of N_v on the triaxiality of the small strain tensor $\boldsymbol{\varepsilon}$ is still not well known (cf. the discussion on $N_v(\boldsymbol{\varepsilon})$ in the Supplementary Material).

5. Conclusion

In conclusion we have devised an experimental set-up that allows to measure the effect of uniform strain on the dark current-voltage characteristic of a solar cell. We observe a reversible effect and use a two-exponential description to obtain the strain-induced change in the diffusion saturation current, which shows a decrease of the order of 3% for a tensile strain with a longitudinal component of 6.8×10^{-4}. We compare this value with that predicted by a model of the *p-n* heterojunction that accounts for strain-dependent carrier mobilities, band energy levels and densities of states. Specifically, the model predicts, for the strain state encountered in the experiment, a decrease in the diffusion saturation current of about 6%. This prediction is in agreement with experiments within a factor of two, a discrepancy that is likely due to the incomplete knowledge of the effect of strain on the density of states of the valence band.

Finally, note that in this work, we have investigated the strain effect on SHJ solar cells, a technology with relatively thick silicon (270 μm), which limits the maximum reachable strain at typically 1×10^{-3}. At these levels of strain, the change in the current-voltage characteristic is measurable but small (a few percent), suggesting that the behavior of the cell is not strongly affected by strain. By contrast, the strain effect could be significantly larger with the higher levels of strain that may be reached in thinner crystalline solar cell technologies (Bergmann, 1999; Chopra et al., 2004), thus motivating further investigations.

Declaration of Competing Interest

The authors declare that they have no known competing financial interests or personal relationships that could have appeared to influence the work reported in this paper.

Acknowledgments

L. Guin thanks W. Chen for his help for the fabrication of the solar cells and V. De Greef for suggesting the loading set-up. This work was supported by the “IDI 2015” project funded by the IDEX Paris-Saclay, ANR-11-IDEX-0003-02.

Appendix A. Supplementary material

Supplementary data associated with this article can be found, in the online version, at https://doi.org/10.1016/j.solener.2019.12.037.

References

Bardeen, J., Shockley, W., 1950. Deformation potentials and mobilities in non-polar crystals. Phys. Rev. 80, 72–80. https://doi.org/10.1103/physrev.80.72.

Bergmann, R., 1999. Crystalline si thin-film solar cells: a review. Appl. Phys. A: Mater. Sci. Process. 69, 187–194. https://doi.org/10.1007/s003390050989.

Bir, G.L., Pikus, G.E., Shelnitz, P., Louvish, D., 1974. Symmetry and Strain-induced Effects in Semiconductors, vol. 624 Wiley, New York.

Chen, A., Yossef, M., Zhang, C., 2018. Strain effect on the performance of amorphous silicon and perovskite solar cells. Sol. Energy 163, 243–250. https://doi.org/10.1016/j.solener.2018.01.057.

Chopra, K.L., Paulson, P.D., Dutta, V., 2004. Thin-film solar cells: an overview. Prog. Photovoltaics Res. Appl. 12, 69–92. https://doi.org/10.1002/pip.541.

Creemer, J., French, P., 2000. The piezojunction effect in bipolar transistors at moderate stress levels: a theoretical and experimental study. Sensors Actuators A: Phys. 82, 181–185. https://doi.org/10.1016/S0924-4247(99)00362-3.

Creemer, J.F., 2002. The Effect of Mechanical Stress on Bipolar Transistor Characteristics (Ph.D. thesis). Delft University of Technology. URL: http://resolver.tudelft.nl/uuid:ff17cb76-7599-486b-b287-3123c806ac0f.

Creemer, J.F., Fruett, F., Meijer, G.C.M., French, P.J., 2001. The piezojunction effect in silicon sensors and circuits and its relation to piezoresistance. IEEE Sens. J. 1, 98. https://doi.org/10.1109/JSEN.2001.936927.

Dai, Y., Huang, Y., He, X., Hui, D., Bai, Y., 2019. Continuous performance assessment of thin-film flexible photovoltaic cells under mechanical loading for building integration. Sol. Energy 183, 96–104. https://doi.org/10.1016/j.solener.2019.03.018.

Fischetti, M.V., Laux, S.E., 1996. Band structure, deformation potentials, and carrier mobility in strained Si, Ge, and SiGe alloys. J. Appl. Phys. 80, 2234. https://doi.org/10.1063/1.363052.

Fonash, S., 2012. Solar Cell Device Physics. Elsevierhttps://doi.org/10.1016/C2009-0-19749-0.

Gleskova, H., Cheng, I.C., Wagner, S., Sturm, J.C., Suo, Z., 2006. Mechanics of thin-film transistors and solar cells on flexible substrates. Sol. Energy 80, 687–693. https://doi.org/10.1016/j.solener.2005.10.010.

Guin, L., 2018. Electromechanical Couplings and Growth Instabilities in Semiconductors (Ph.D. thesis). Université Paris-Saclay - Ecole polytechnique. URL: https://tel.archives-ouvertes.fr/tel-02124459.

Guin, L., Jabbour, M., Triantafyllidis, N., 2018. The p-n junction under nonuniform strains: general theory and application to photovoltaics. J. Mech. Phys. Solids 110, 54–79. https://doi.org/10.1016/j.jmps.2017.09.004.

Herring, C., Vogt, E., 1956. Transport and deformation-potential theory for many-valley semiconductors with anisotropic scattering. Phys. Rev. 101, 944–961. https://doi.org/10.1103/physrev.101.944.

Imai, T., Uchida, M., Sato, H., Kobayashi, A., 1965. Effect of uniaxial stress on germanium p-n Junctions. Jpn. J. Appl. Phys. 4, 102–113. https://doi.org/10.1143/jjap.4.102.

Jones, R., Johnson, T., Jordan, W., Wagner, S., Yang, J., Guha, S., 2002. Effects of mechanical strain on the performance of amorphous silicon triple-junction solar cells. In: Conference Record of the Twenty-Ninth IEEE Photovoltaic Specialists Conference, 2002, pp. 1214–1217. http://doi.org/10.1109/PVSC.2002.1190826.

Kanda, Y., 1967. Effect of stress on germanium and silicon p-n junctions. Jpn. J. Appl. Phys. 6, 475. https://doi.org/10.1143/JJAP.6.475.

Kanda, Y., 1991. Piezoresistance effect of silicon. Sensors Actuators A: Phys. 28, 83–91. https://doi.org/10.1016/0924-4247(91)85017-i.

Kleimann, P., Semmache, B., Le Berre, M., Barbier, D., 1998. Stress-dependent hole effective masses and piezoresistive properties of p-type monocrystalline and polycrystalline silicon. Phys. Rev. B 57, 8966–8971. https://doi.org/10.1103/PhysRevB.57.8966.

Lange, D., Roca i Cabarrocas, P., Triantafyllidis, N., Daineka, D., 2016. Piezoresistivity of thin film semiconductors with application to thin film silicon solar cells. Sol. Energy Mater. Sol. Cells 145 (Part 2), 93–103.

Nelson, J., 2003. The Physics of Solar Cells, vol. 1 Imperial College Press, UK doi:10.1142/p276.

Pagliaro, M., Ciriminna, R., Palmisano, G., 2008. Flexible solar cells. ChemSusChem 1, 880–891. https://doi.org/10.1002/cssc.200800127.

Rindner, W., 1965. Effects of uniaxial and inhomogeneous stress in germanium and silicon p-n junctions. J. Appl. Phys. 36, 2513–2518. https://doi.org/10.1063/1.1714521.

Rueda, H.A., 1999. Modeling of Mechanical Stress in Silicon Isolation Technology and its Influence on Device Characteristics (Ph.D. thesis). URL: http://swamp.mse.ufl.edu/dissertations/rueda_h.pdf.

Smith, C.S., 1954. Piezoresistance effect in germanium and silicon. Phys. Rev. 94, 42–49. https://doi.org/10.1103/physrev.94.42.

Suckow, S., 2014. 2/3-diode fit. URL: https://nanohub.org/resources/14300.

Suckow, S., Pletzer, T.M., Kurz, H., 2012. Fast and reliable calculation of the two-diode model without simplifications. Prog. Photovoltaics Res. Appl. 22, 494–501. https://doi.org/10.1002/pip.2301.

Sze, S.M., Ng, K.K., 2006. Physics of Semiconductor Devices. John Wiley & Sons. https://doi.org/10.1002/0470068329.

Taguchi, M., Maruyama, E., Tanaka, M., 2008. Temperature dependence of amorphous/crystalline silicon heterojunction solar cells. Jpn. J. Appl. Phys. 47, 814–818. https://doi.org/10.1143/jjap.47.814.

Velut, P., Tween, R., Teuscher, R., Leterrier, Y., Månson, J.A.E., Galliano, F., Fischer, D., 2014. Conformal thin film silicon photovoltaic modules. Int. J. Sustain. Energ. 33, 783–796. https://doi.org/10.1080/14786451.2013.766611.

Wolf, M., Noel, G., Stirn, R., 1977. Investigation of the double exponential in the current—voltage characteristics of silicon solar cells. IEEE Trans. Electron Devices 24, 419–428. https://doi.org/10.1109/t-ed.1977.18750.

Wooten, F.T., Brooks, A.D., Wortman, J.J., 1968. Effect of uniform stress on si p-n junctions. Proc. IEEE 56, 1221–1222. https://doi.org/10.1109/PROC.1968.6527.

Wortman, J.J., Evans, R.A., 1965. Young’s modulus, shear modulus, and poisson’s ratio in silicon and germanium. J. Appl. Phys. 36, 153. https://doi.org/10.1063/1.1713863.

Wortman, J.J., Hauser, J.R., 1966. Effect of mechanical stress on p-n junction device characteristics. ii. generation-recombination current. J. Appl. Phys. 37, 3527–3530. https://doi.org/10.1063/1.1708894.

Wortman, J.J., Hauser, J.R., Burger, R.M., 1964. Effect of mechanical stress on p-n junction device characteristics. J. Appl. Phys. 35, 2122–2131. https://doi.org/10.1063/1.1702802.

Supplementary material: effect of strain on the dark current-voltage characteristic of silicon heterojunction solar cells

L. Guin,[1,2] P. Roca i Cabarrocas,[2] M. E. Jabbour,[1,3] and N. Triantafyllidis[1,3,4]
[1)] *LMS, École polytechnique, CNRS, Institut polytechnique de Paris, 91128 Palaiseau, France*
[2)] *LPICM, École polytechnique, CNRS, Institut polytechnique de Paris, 91128 Palaiseau, France*
[3)] *Département de Mécanique, École polytechnique, 91128 Palaiseau, France*
[4)] *Aerospace Engineering Department & Mechanical Engineering Department (emeritus), The University of Michigan, Ann Arbor, MI 48109-2140, USA*

In this supplementary material, we present the strain dependence of the electronic parameters of silicon for an arbitrary strain triaxiality. To this end, we use the results from the solid state physics literature on the dependence on strain of the properties of the subbands of the conduction and valence bands of silicon to derive an equivalent two-band formulation for the effective strain dependence of the band edges and densities of states. In sum, we derive the following quantities:

$$\begin{cases} \Delta E_c(\boldsymbol{\varepsilon}) = E_c(\boldsymbol{\varepsilon}) - E_c^r, & \Delta E_v(\boldsymbol{\varepsilon}) = E_v(\boldsymbol{\varepsilon}) - E_v^r, \\ \Delta N_c(\boldsymbol{\varepsilon}) = N_c(\boldsymbol{\varepsilon}) - N_c^r, & \Delta N_v(\boldsymbol{\varepsilon}) = N_v(\boldsymbol{\varepsilon}) - N_v^r, \end{cases} \tag{S1}$$

as well as the changes in the rank-2 tensorial mobilities,

$$\Delta \mathbf{M}_n(\boldsymbol{\varepsilon}) = \mathbf{M}_n(\boldsymbol{\varepsilon}) - \mathbf{M}_n^r, \qquad \Delta \mathbf{M}_p(\boldsymbol{\varepsilon}) = \mathbf{M}_p(\boldsymbol{\varepsilon}) - \mathbf{M}_p^r, \tag{S2}$$

where the superscript r denotes the relaxed state of the crystal ($\boldsymbol{\varepsilon} = \mathbf{0}$).

I. REDUCTION OF THE BAND STRUCTURE TO A TWO BANDS DESCRIPTION

The energy band structure of silicon has six subbands in the conduction band and two subbands—called heavy hole band and light hole band—in the valence band (a third subband of the valence band, called spin-orbit band, can be neglected as justified subsequently). Band structure computations performed on the strained crystal allows to quantify the strain-induced changes in each subband. In this section, we shall reduce the multiple band picture of solid state physics to a simplified description with one effective conduction band and one effective valence band, with strain-induced changes equivalent to the compiled effects on the subbands.

A. Conduction band

First, consider the conduction band of silicon. Its six subbands have, in the relaxed state, equal Density Of States (DOS), denoted by $N_{sc,r}$ (the index *sc* indicates a Subband of the Conduction band and r the Relaxed state $\boldsymbol{\varepsilon} = \mathbf{0}$), and equal edge energy corresponding to the edge energy of the effective conduction band $E_{c,r}$. Under an applied small strain $\boldsymbol{\varepsilon}$, the edge energy of the m conduction subband changes by the quantity $\Delta E_{sc}^m(\boldsymbol{\varepsilon})$, while the change in effective density of states is much smaller and can be neglected.[S1] The computation of the change in band edge $\Delta E_{sc}^m(\boldsymbol{\varepsilon})$ is treated with the deformation potential theory that was introduced by Bardeen and Shockley[S2] and further developed in Refs. S3 and S4. It is usually modeled with the *dilational deformation potential* Ξ_d and *shear deformation potential* Ξ_u by:

$$\Delta E_{sc}^m(\boldsymbol{\varepsilon}) = (\Xi_d \mathbf{I} + \Xi_u \mathbf{k}^m \otimes \mathbf{k}^m) : \boldsymbol{\varepsilon}, \tag{S3}$$

where $\mathbf{k}^m$ is the unit vector associated to the direction of the band m in the $\mathbf{k}$-space (reciprocal to the physical space).

Let $\mathscr{B}_M = (\mathbf{e}_1, \mathbf{e}_2, \mathbf{e}_3)$, the basis aligned with the principal crystallographic directions $\langle 100 \rangle$ of silicon (index M of $\mathscr{B}_M$ is for material, as it is attached to the directions of the material), the $\mathbf{k}^m$ vectors are $\pm\mathbf{e}_1, \pm\mathbf{e}_2, \pm\mathbf{e}_3$ for the subbands $m = 1,4$, $m = 2,5$, and $m = 3,6$, respectively. Values for Ξ_d and Ξ_u vary in the literature by about 10 %. We take the values from Ref. S3: $\Xi_d = 1.1$ eV and $\Xi_u = 10.5$ eV.

We now introduce a unique effective conduction band with DOS N_c and edge energy $E_c(\boldsymbol{\varepsilon})$. These properties—and their strain dependence—are determined by the equality, at first order in strain, of the expressions of density of electron in the effective band description and in the multiple-band model.

In the multiple-band description, the density of electrons $n(\varepsilon)$ is given by[S5]

$$n(\varepsilon) = \sum_{m=1}^{6} N_{sc} \exp\Big[-\big(E_c^r + \Delta E_{sc}^m(\varepsilon) - E_{F_n}(\varepsilon)\big)/k_B T\Big], \tag{S4}$$

where $E_{F_n}(\varepsilon)$ is the quasi-Fermi level for electrons. Likewise, in the one-band description, the density of electrons reads

$$n(\varepsilon) = N_c \exp\Big[-\big(E_c^r + \Delta E_c(\varepsilon) - E_{F_n}(\varepsilon)\big)/k_B T\Big]. \tag{S5}$$

By letting,

$$N_c = 6N_{sc}, \qquad \Delta E_c(\varepsilon) = -k_B T \ln\left(\frac{1}{6}\sum_{m=1}^{6} \exp\big[-\Delta E_{sc}^m(\varepsilon)/k_B T\big]\right), \tag{S6}$$

the equality of electron densities in the two descriptions Eq. (S4) and Eq. (S5) is satisfied. With the aim of developing a first order linear theory of the effect of strain on semiconductors, we linearize Eq. (S6) for small strain-induced changes:

$$\Delta E_c(\varepsilon) = \frac{1}{6}\sum_{m=1}^{6} \Delta E_{sc}^m(\varepsilon). \tag{S7}$$

Finally, inserting Eq. (S3) in Eq. (S7) yields

$$\Delta E_c(\varepsilon) = \Big(\Xi_d + \frac{1}{3}\Xi_u\Big)\mathbf{I} : \varepsilon. \tag{S8}$$

B. Valence band

Second, consider the valence band comprised of the heavy hole band and light hole band. While these two bands have the same energy level in the relaxed state, there also exists a third subband, the spin-orbit coupling band, lying at a lower energy level than the two others. As such, this subband contributes much less to the density of holes and can be neglected. In the same way as for the conduction band, we derive an equivalent one-band description with the additional difficulty that the densities of states of the heavy and light hole bands depend significantly on strain.

Denote by $\Delta E_{sv}^l(\varepsilon)$ and $\Delta E_{sv}^h(\varepsilon)$ the changes in band edge energy of the light and heavy hole subbands with respect to their common level in the relaxed state E_v^r and let $\Delta N_{sv}^l(\varepsilon)$ and $\Delta N_{sv}^h(\varepsilon)$ the changes in DOS of these two subbands. In the multiple-band description, the density of holes $p(\varepsilon)$ is given by

$$\begin{aligned} p(\varepsilon) = \Big(\Big(N_{sv,r}^l + \Delta N_{sv}^l(\varepsilon)\Big)\exp\Big[\Delta E_{sv}^l(\varepsilon)/k_B T\Big] + \Big(N_{sv,r}^h + \Delta N_{sv}^h(\varepsilon)\Big)\exp\Big[\Delta E_{sv}^h(\varepsilon)/k_B T\Big]\Big) \times \\ \exp\Big[\big(E_v^r - E_{F_p}(\varepsilon)\big)/k_B T\Big], \end{aligned} \tag{S9}$$

where $E_{F_p}(\varepsilon)$ is the quasi-Fermi level of holes.

In the one-band description of the valence band, the density of holes reads

$$p(\varepsilon) = \Big(N_v^r + \Delta N_v(\varepsilon)\Big)\exp\big[(E_v^r + \Delta E_v(\varepsilon) - E_{F_p}(\varepsilon))/k_B T\big], \tag{S10}$$

where $\Delta N_v(\varepsilon)$ and $\Delta E_v(\varepsilon)$ are the effective change of the one-band density of states and energy level to be computed from the knowledge on the subbands. Equality of Eq. (S9) and Eq. (S10) yields, at first order in ε,

$$\begin{aligned} \Delta N_v(\varepsilon) &= \Delta N_{sv}^l(\varepsilon) + \Delta N_{sv}^h(\varepsilon), \\ \Delta E_v(\varepsilon) &= \frac{N_{sv,r}^l}{N_v^r}\Delta E_{sv}^l(\varepsilon) + \frac{N_{sv,r}^h}{N_v^r}\Delta E_{sv}^h(\varepsilon). \end{aligned} \tag{S11}$$

In sum, the strain dependence of the equivalent one-band quantities has been expressed as function of the strain dependence of the subband quantities. The latter can be found in the solid state physics literature, in particular the change in subband energy level is given by Kanda[S6], for $u = h, l$,

$$\Delta E_{sv}^u(\varepsilon) = a\mathbf{I} : \varepsilon \pm \left(\frac{b^2}{2}\big((\varepsilon_{11}-\varepsilon_{22})^2 + (\varepsilon_{11}-\varepsilon_{33})^2 + (\varepsilon_{33}-\varepsilon_{22})^2\big) + d^2\big(\varepsilon_{12}^2 + \varepsilon_{13}^2 + \varepsilon_{23}^2\big)\right)^{1/2}, \tag{S12}$$

where the the plus sign is for the heavy hole band and the minus sign for the light hole band[S1] and a, b and d are the valence band deformation potentials for which we retain the most recent values from Ref. S7: $a = 2.1\,\mathrm{eV}$, $b = -2.33\,\mathrm{eV}$ and $d = -4.75\,\mathrm{eV}$. For the effective description of the valence band, $\Delta E_v(\varepsilon)$ is obtained combining Eq. (S11) and Eq. (S12) with $N^h_{sv,r}/N^r_v = 0.84$ and $N^l_{sv,r}/N^r_v = 0.16$.[S8]

While it has been recognized early that, unlike the conduction band, the effective density of states of the valence band depends on strain[S4,S6,S9] it is only recently that Creemer[S1] pointed out that the change in DOS of the valence band contributes significantly to the piezojunction effect, in particular at relatively moderate strains (a few tenth of percent). We do not have an analytical expression valid for an arbitrary triaxial strain state of that strain dependence and therefore assume an hydrostatic relation, which we calibrate from the band calculations under uniaxial strain of Ref. S1. In addition, these band calculations reflect a symmetric behavior between tensile and compressive strains, which we account for. The hydrostatic strain dependence is a strong assumption and we should, in the following, keep in mind that the estimated contribution to the change in electric current induced by the modification of the valence band density of states is very uncertain. In sum, we write, for each valence subband $u = h, l$,

$$\Delta N^u_{sv}(\varepsilon) = \widetilde{N}^u_{sv}\,|\mathbf{I} : \varepsilon|, \tag{S13}$$

where the scalar coefficients $\widetilde{N}^l_{sv} = 240 N^l_{sv,r}$ and $\widetilde{N}^h_{sv} = -240 N^h_{sv,r}$ are computed from Figure 2.16 of Ref. S1. Combining Eq. (S11) with Eq. (S13), we obtain the strain dependence of the effective valence band density of states:

$$\Delta N_v(\varepsilon) = \widetilde{N}_v\,|\mathbf{I} : \varepsilon|, \tag{S14}$$

with $\widetilde{N}_v = -170 N^r_v$. Relation Eq. (S14) is only an approximate estimation of the strain effect on the DOS of the valence band. A detailed band calculation for general strain is required to derive a more exact strain dependence with full account of strain triaxiality.

II. CHANGE IN MOBILITIES

A. General Theory

The change with strain of the mobility of electrons and holes is equal to the opposite of the change in resistivity. The latter is measured in experiments[S1,S10] and, as such, yields the mobility changes of electrons and holes in the effective one-band description. Thus, there is no need to resort to the subband description for mobilities. The changes in resistivity are usually expressed with respect to the stress tensor $\boldsymbol{\sigma}$ with the rank-4 piezoresistive tensors $\boldsymbol{\Pi}_n$ and $\boldsymbol{\Pi}_p$ for electrons and holes.[S1,S10,S11] Using those tensors and the constitutive relation $\boldsymbol{\sigma} = \mathbf{c} : \varepsilon$ with $\mathbf{c}$ the elasticity tensor, the relative change in the ij-coefficient of the mobility tensor can be expressed with the small strain tensor ε

$$\frac{(\Delta \mathbf{M}_q)_{ij}(\varepsilon)}{(\mathbf{M}^r_q)_{ij}} = -\big(\boldsymbol{\Pi}_q : \mathbf{c} : \varepsilon\big)_{ij}, \tag{S15}$$

for $q = n, p$ and for every $i, j = 1, 2, 3$, without summation on the repeated indices.

a. Practical calculation of the effect of strain on mobilities Equation. (S15) can be expressed in matrix form using the Voigt notation. Denote by $[\mathbf{a}]^{\mathscr{B}}$ the matrix of the coefficients of a tensor $\mathbf{a}$ of rank-1 or -2 in the basis $\mathscr{B}$ and $\{\mathbf{A}\}^{\mathscr{B}}$ the representation, *in Voigt notation*, of a properly symmetric tensor $\mathbf{A}$ of rank-2 or -4 in basis $\mathscr{B}$. For any rank-2 tensor, we have the usual relation between classical and Voigt notations,

$$\begin{aligned} \{\mathbf{A}\}_1 = [\mathbf{A}]_{11}, \quad \{\mathbf{A}\}_2 = [\mathbf{A}]_{22}, \quad \{\mathbf{A}\}_3 = [\mathbf{A}]_{33}, \\ \{\mathbf{A}\}_4 = [\mathbf{A}]_{23}, \quad \{\mathbf{A}\}_5 = [\mathbf{A}]_{13}, \quad \{\mathbf{A}\}_6 = [\mathbf{A}]_{12}, \end{aligned} \tag{S16}$$

with an exception for the extradiagonal terms of the strain tensor ε,

$$\{\varepsilon\}_4 = 2[\varepsilon]_{23}, \quad \{\varepsilon\}_5 = 2[\varepsilon]_{13}, \quad \{\varepsilon\}_6 = 2[\varepsilon]_{12}. \tag{S17}$$

This allows us to rewrite Eq. (S15) as

$$\frac{\{\Delta \mathbf{M}_q\}_i(\varepsilon)}{\{\mathbf{M}^r_q\}_i} = -\big(\{\boldsymbol{\Pi}\}_q \cdot \{\mathbf{c}\} \cdot \{\varepsilon\}\big)_i, \tag{S18}$$

Π^n_{11}	Π^n_{12}	Π^n_{44}	Π^p_{11}	Π^p_{12}	Π^p_{44}
-102.2	53.4	-13.6	6.6	-1.1	138.1

TABLE I. Piezoresistive coefficients in 10^{-11} Pa^{-1} from Ref. S10. For comparison with values obtained by other works see Ref. S1, Table 2.4.

for every $i = 1..6$, where for two rank-2 or -4 tensors $\mathbf{A}$ and $\mathbf{B}$, $\{\mathbf{A}\}\cdot\{\mathbf{B}\}$ denotes the traditional matrix-matrix or matrix-vector product.

In Voigt notations, due to the cubic symmetries of silicon, in the basis $\mathscr{B}_M$, the matrices $\{\mathbf{\Pi}_q\}$ for $q = n, p$ read[S10–S12]

$$\{\mathbf{\Pi}_q\}^{\mathscr{B}_M} = \begin{pmatrix} \Pi^q_{11} & \Pi^q_{12} & \Pi^q_{12} & 0 & 0 & 0 \\ \Pi^q_{12} & \Pi^q_{11} & \Pi^q_{12} & 0 & 0 & 0 \\ \Pi^q_{12} & \Pi^q_{12} & \Pi^q_{11} & 0 & 0 & 0 \\ 0 & 0 & 0 & \Pi^q_{44} & 0 & 0 \\ 0 & 0 & 0 & 0 & \Pi^q_{44} & 0 \\ 0 & 0 & 0 & 0 & 0 & \Pi^q_{44} \end{pmatrix}, \tag{S19}$$

with the coefficients summarized in Table I. Note the variations up to two orders of magnitude between the different coefficients of Table I, which indicate that the carrier mobilities might be significantly or little affected by the stress depending on both:

1. The stress state (i.e., its triaxiality),
2. The components of the mobility tensor relevant for a particular experiments and which are determined by the directions of electron (resp. hole) current and gradient of electron (resp. hole) electrochemical potential.[S13]

We also recall that the elasticity tensor $\mathbf{c}$ of silicon in Voigt notation has the same form as Eq. (S19) with coefficients in the basis $\mathscr{B}_M$, $c_{11} = 166$ GPa, $c_{12} = 64$ GPa and $c_{44} = 80$ GPa.[S14]

B. Application to the experiment shown in Fig. 2 of the main article

In the following, we show why the strain dependence in the hole mobility can be neglected for the particular crystallographic directions of the experiment reported in Fig. 2 of the main article. With the basis $\mathscr{B}_G$ of Fig. 2, the component of the mobility tensor involved in hole transport is $M_{p,zz}$. The change with strain of that component is computed using Eq. (S18), which yields by taking the component ε_{yy} for the amplitude of strain (ε_{xx} and ε_{zz} are implicitly accounted for by writing them as a function of ε_{yy}):

$$\frac{\Delta M_{p,zz}}{M_{p,zz}} = -\frac{4c_{11}^2 c_{44} + 4c_{11}c_{12}c_{44} - 8c_{12}^2 c_{44}}{c_{11}^2 + c_{11}c_{12} + 2c_{11}c_{44} - 2c_{12}^2}\Pi^p_{12}\varepsilon_{yy}, \tag{S20}$$

Numerically, for $\varepsilon_{yy} = 1 \times 10^{-3}$ (upper bound in the experiments), the relative change in mobility is only of 0.2% which is very small compared to the changes due to the other phenomena (of the order of 10%). As a result, for the experiment under consideration the influence of mobility can be neglected as mentioned in the main article.

[S1]J. F. Creemer, *The effect of mechanical stress on bipolar transistor characteristics*, Ph.D. thesis, Delft University of Technology (2002).

[S2]J. Bardeen and W. Shockley, "Deformation potentials and mobilities in non-polar crystals," Physical Review **80**, 72–80 (1950).

[S3]C. Herring and E. Vogt, "Transport and deformation-potential theory for many-valley semiconductors with anisotropic scattering," Physical Review **101**, 944–961 (1956).

[S4]G. L. Bir, G. E. Pikus, P. Shelnitz, and D. Louvish, *Symmetry and strain-induced effects in semiconductors*, Vol. 624 (Wiley New York, 1974).

[S5]J. J. Wortman, J. R. Hauser, and R. M. Burger, "Effect of mechanical stress on p-n junction device characteristics," Journal of Applied Physics **35**, 2122–2131 (1964).

[S6]Y. Kanda, "Effect of stress on germanium and silicon p-n junctions," Japanese Journal of Applied Physics **6**, 475 (1967).

[S7]M. V. Fischetti and S. E. Laux, "Band structure, deformation potentials, and carrier mobility in strained si, ge, and SiGe alloys," Journal of Applied Physics **80**, 2234 (1996).

[S8]These ratio of density of states are obtained as follows: The effective density of states of each subband is related to the effective mass of each subband m^l and m^h by[S15]

$$N^u_{sv,r} \propto (m^u)^{3/2}, \tag{S21}$$

for $u = l, h$ where $m^l = 0.16m_0$ and $m^h = 0.49m_0$ with m_0 the free-electron mass. In addition, the density of states of the effective valence band is simply,

$$N^r_v = N^l_{sv,r} + N^h_{sv,r}, \tag{S22}$$

which combined with Eq. (S21) yields the ratios of DOS.

[S9]P. Kleimann, B. Semmache, M. Le Berre, and D. Barbier, "Stress-dependent hole effective masses and piezoresistive properties of p-type monocrystalline and polycrystalline silicon," Phys. Rev. B **57**, 8966–8971 (1998).
[S10]C. S. Smith, "Piezoresistance effect in germanium and silicon," Physical Review **94**, 42–49 (1954).
[S11]Y. Kanda, "A graphical representation of the piezoresistance coefficients in silicon," IEEE Transactions on Electron Devices **29**, 64–70 (1982).
[S12]Y. Sun, S. E. Thompson, and T. Nishida, *Strain Effect in Semiconductors* (Springer Nature, 2010).
[S13]L. Guin, M. Jabbour, and N. Triantafyllidis, "The p-n junction under nonuniform strains: general theory and application to photovoltaics," Journal of the Mechanics and Physics of Solids **110**, 54–79 (2018).
[S14]J. J. Wortman and R. A. Evans, "Young's modulus, shear modulus, and poisson's ratio in silicon and germanium," Journal of Applied Physics **36**, 153 (1965).
[S15]S. M. Sze and K. K. Ng, *Physics of semiconductor devices* (John wiley & sons, 2006).